ESD TDR 64-19

ESTI FILE COPY

ESD-TDR-64-19

ESAT PROCESSED
ESD CONTROL NR AL-32697
DATE RECEIVED
CY NR. 1 OF 1 CYS

Group Report 1964-3

A. F. Smith

Radar Backscatter from Some Low Cross-Section Shapes

16 January 1964

Prepared under Electronic Systems Division Contract AF 19(628)-500 by

Lincoln Laboratory
MASSACHUSETTS INSTITUTE OF TECHNOLOGY
Lexington, Massachusetts

AD0431780

The work reported in this document was performed at Lincoln Laboratory, a center for research operated by Massachusetts Institute of Technology, with the support of the U.S. Air Force under Contract AF 19(628)-500.

NOTICE: When government or other drawings, specifications or other data are used for any purpose other than in connection with a definitely related government procurement operation, the U. S. Government thereby incurs no responsibility, nor any obligation whatsoever; and the fact that the Government may have formulated, furnished, or in any way supplied the said drawings, specifications, or other data is not to be regarded by implication or otherwise as in any manner licensing the holder or any other person or corporation, or conveying any rights or permission to manufacture, use or sell any patented invention that may in any way be related thereto.

UNCLASSIFIED

AD 431780

DEFENSE DOCUMENTATION CENTER

FOR

SCIENTIFIC AND TECHNICAL INFORMATION

CAMERON STATION, ALEXANDRIA, VIRGINIA

UNCLASSIFIED

MASSACHUSETTS INSTITUTE OF TECHNOLOGY

LINCOLN LABORATORY

RADAR BACKSCATTER FROM SOME LOW CROSS-SECTION SHAPES

A. F. SMITH

Group 22

GROUP REPORT 1964-3

16 JANUARY 1964

LEXINGTON MASSACHUSETTS

ABSTRACT

Radar backscattering measurements have been made on four low cross-section shapes. Results indicate that little improvement is found over the return from a cone-sphere. Comparison of measured data with approximate theoretical calculations shows fair agreement.

This technical documentary report is approved for distribution.

Franklin C. Hudson, Deputy Chief
Air Force Lincoln Laboratory Office

TABLE OF CONTENTS

ABSTRACT		iii
I.	INTRODUCTION	1
II.	THE MODELS	2
III.	THE MEASUREMENTS	3
IV.	THE MEASURED DATA	5
V.	COMPARISON OF MEASURED DATA WITH APPROXIMATE THEORETICAL CALCULATIONS	7
VI.	CONCLUSIONS	8
REFERENCES		9

TABLES

TABLE I: MEASURED DATA 4

I. INTRODUCTION

There is considerable interest in reducing the radar backscattering from axisymmetric conducting bodies over some specified range of aspect angles* (say within 45^{o} of the nose-on aspect). Perhaps the simplest means for achieving this end is shaping. By proper shaping, specular reflections can be avoided, and traveling wave and creeping wave return can be lowered.

The cone-sphere is a low cross-section shape which has received much attention[1,2,3,4,5]. The conical forebody prevents specular returns at aspects within $\pm (90^{o} - \alpha)$ from nose-on, where α is the cone half-angle. In addition, the surface has continuous first derivatives, except for the tip, so that the return associated with waves traveling along the surface and reflected by discontinuities in surface derivatives, usually called the "traveling wave" return, is reduced. There is, of course, a discontinuity in the second surface derivative (or, equivalently, the curvature) at the junction of the cone and spherical cap, so that some traveling wave return is still present. Backscattering from the tip can be shown to be negligible in comparison to the measured scattering from the cone-sphere.

In addition to the traveling wave, the other major contributor to the near nose-on backscattering from the cone-sphere is the "creeping wave" return. This return is attributed to waves which are launched in the penumbra region** and which move or "creep" around the shadowed region of the body and reappear on the opposite side to direct energy toward the receiver.

The objective of the measurements reported herein was to investigate experimentally the scattering from a number of shapes somewhat more sophisticated in

---

*The aspect angle is the angle between the body symmetry axis and the direction of propagation of the incident wave.

**The region containing the boundary between the portion of the body directly illuminated by the incident wave and the shadowed region.

concept than the cone-sphere to determine if a significant reduction in near nose-on cross section could be attained. Three of these shapes, FOXTROT, GOLF, and KING, were designed to lower traveling wave return by reducing discontinuities in surface derivatives higher than the first. The fourth model, JULIET, was designed to determine the effect of a back-end modification on the creeping wave return.

II. THE MODELS

Each of the four shapes is described below. They are shown in Figs. 1 through 4 and compared in Fig. 5. Each shape is axisymmetric and, thus, is obtained by rotating a generating contour about an axis of symmetry; the models will be described in terms of these contours.

The generating contour for FOXTROT is shown in Fig. 1. The forward and rear contours are both segments of circles, which generate an ogival forward section and a spherical rear cap. The ogive and sphere are tangent at the junction but differ in their second derivatives, thus producing, as with the cone-sphere, a finite discontinuity in the second surface derivative, but of smaller magnitude than that of a comparable cone-sphere.

The contour for GOLF is shown in Fig. 2. The forward section is a straight line (thus generating a cone), the mid-section is a quartic curve, and the rear section is a segment of an ellipse. Both first and second derivatives are continuous at the junction of the constituent curves.

The contour for JULIET (Fig. 3) is identical to that for GOLF in the forward and mid-sections. The rear section is also generated by an ellipse, as for GOLF, but the center is offset to produce a re-entrant back end. Both first and second derivatives are continuous where the curves join.

The generating contour for KING is shown in Fig. 4. It is calculated using an equation of the form

$$r = b\,(\cos n\theta)^m, \quad \left(0 \le \theta \le \frac{\pi}{2n}\right).$$

where the equation is in polar coordinates (r, θ), with the origin at the tip of the shape, and θ is measured from the symmetry axis. The constants b, m, and n are parameters determining the size and shape of the body. Thus it can be seen that there are no discontinuities in the surface derivatives of any order, except, as for all four shapes, at the tip. Note, in Fig. 5, that although the contours for GOLF and KING were determined by different equations, the forward contours are virtually indistinguishable when drawn to this scale.

III. THE MEASUREMENTS

Metallic models of the shapes described above have been made in a number of sizes and measured at several frequencies for both horizontal and vertical polarization. (See Table I.) The measurement facilities included those of the Defense Research Telecommunications Establishment of Canada (DRTE); Radiation, Incorporated (Rad.); The Cornell Aeronautical Laboratory (CAL); General Dynamics/Fort Worth (GD/FW); The Conductron Corporation (Cond.); and Lincoln Laboratory (L.L.).

At all facilities except that of CAL the models were supported by styrofoam columns and rotated about an axis perpendicular to the plane of the symmetry axis and the radar beam axis. At CAL a string support system was used.

Background return (including column return) was measured before and after each model measurement at Radiation, Inc., Conductron, and Lincoln Laboratory. At GD/FW, background return (which is quite stable there) was monitored between runs but was only recorded before and after each day's series of measurements. The background data available from DRTE consists of a measured background for each of the measurements at 35,000 Mc. and a quoted value of average background return for the X-band (9000 Mc) data. Because a string support system was used at CAL, it was not possible to measure the return of the supporting system without the model present. However, estimated peak values of background return calculated from string data have been provided by CAL for the more important case of vertical polarization.

From the available background data, estimates of average background return in the region $\pm 45^{\circ}$ from nose-on have been made for each model measurement (except those from CAL). These values are given in Table I.

Model	Meas. Facility	Scale	Meas. Freq. (Mc)	a/λ	Pol.	σ Ave ($\pm 45^{o}_{2}$) (db λ^{2})	Bckgrd Ave ($\pm 45^{o}_{2}$) (db λ^{2})
FOXTROT	DRTE	1.0	9,000	1.05	HH VV	-12.1 - 8.3	-35* -35*
	L.L.	0.5	35,000	2.04	HH	-14.0	-24
	DRTE	1.0	35,000	4.08	HH VV	- 5 -11	- 6 -14
GOLF	Cond.	1.0	8,500	1.08	HH VV	-17.2 -11.2	<-29 <-30
	DRTE	1.0	9,000	1.14	HH VV	-14.9 -10.8	-35* -35*
	Cond.	1.0	9,600	1.22	HH VV	-13.4 -11.9	-22.5 -25
	Rad.	2.0	9,600	2.44	HH VV	-24.0 -15.6	-26 <-30
	DRTE	1.0	35,000	4.45	HH VV	- 8 -11	-11 - 9
JULIET	Rad.	1.0	9,600	1.22	HH VV	-15.6 -10.1	-28 <-29
	CAL	1.0	35,000	4.45	HH VV	-15.9 -16.9	-- --
KING	Cond.	1.0	8,500	1.08	HH VV	-15.8 -11.3	<-26 <-29
			9,600	1.22	HH VV	-16.1 -12.8	-28 -23
	GD/FW	2.0	4,800	1.22	HH VV	-13.1 -10.6	-23 -27
			9,600	2.44	HH VV	-18.6 -22.1	-31 -31

*DRTE statement, no recorded data available

TABLE I

In conjunction with their measurement program for JULIET, CAL made an investigation of the effect of model orientation and position, relative to the radar beam axis, on measured cross sections. It was found that the angular orientation in pitch or tilt (ideally 0^{o}) had a profound effect on the amplitude and position of the lobes in the nose-on region. Since this angular alignment is particularly hard to control with a string support system, they concluded that this accounted for the day to day variation noted in successive patterns obtained on model JULIET. It is probable also that angular misorientation is responsible for at least some of the difficulties encountered in obtaining satisfactory patterns at the other installations. At Lincoln Laboratory, for example, it was found that a symmetric pattern for FOXTROT could be obtained only after precision optical alignment of the model.

IV. THE MEASURED DATA

The patterns of cross section vs. aspect angle obtained on models FOXTROT, GOLF, JULIET, and KING are shown in Figs. 6 to 20. The cross-section values are given in $db\lambda^{2}$.*

Average cross-section values have been calculated (by a numerical integration of cross section in square wavelengths) over the region $\pm 45^{o}$ from nose-on. These are tabulated in Table I. In Fig. 21 these values are plotted vs. a/λ. where a is the maximum radius of the body. Also plotted in Fig. 21 are the estimated values of background return for each measurement and (for comparison purposes) a curve showing the trend of cross-section data obtained earlier and reported elsewhere[3] on model INDIA--a cone-sphere with 12.5^{o} cone half-angle. Note that in the region where $0.5 < (a/\lambda) < 2$ the "low cross-section" shapes show average nose-on returns comparable to those of the cone-sphere shape. At higher values of a/λ the "low cross-section" shapes appear to show slightly lower averages, but the data are insufficient to warrant drawing definite conclusions.

Recent theoretical calculations[3] have shown that for the cone-sphere the magnitudes of the traveling return and the creeping wave return in the near nose-on region are

*decibels relative to a square wavelength (λ^{2}), where λ is the wavelength of the incident radiation.

comparable for values of a/λ near 3; at higher values the traveling wave return is dominant, and at lower values the creeping wave return is dominant. Most of the data presented have been obtained in the range $(a/\lambda) < 3$, i.e., that region where the creeping wave dominates the backscattering return for cone-sphere shapes. Since models FOXTROT, GOLF, and KING were designed to reduce traveling wave return, it is not surprising, then, that a large reduction over the cone-sphere cross section is not observed for these shapes. However, values of average cross section for JULIET, designed similarly to GOLF, but with a re-entrant back-end to attempt to perturb the creeping wave, also show no striking reduction.

Note that the patterns obtained (Figs. 6 to 20) show varying degrees of symmetry (symmetry being an indication of validity for these measurements on axisymmetric models). It is true that those patterns showing good symmetry correspond to measurements where the average background return was at least 10 db and, in general, near 20 db below the average measured model return over $\pm 45^{\circ}$ from nose-on. Also, patterns where the average background was less than 10 db below the average measured model return show poor symmetry properties. There are, however, some patterns with average background level 10 db or more below the measured model level which also show poor symmetry. It has not been possible to ascertain the reason for this, but, as indicated in Section III, it is probable that angular misorientation of the model is responsible to some degree. Possible also are multiple bounce effects and other interactions between the model and the model support system.

On the JULIET patterns obtained at CAL at 35,000 Mc (Figs. 15 and 16) large lobes are noted at aspects of approximately $\pm 36^{\circ} - 40^{\circ}$ and $\pm 51^{\circ} - 56^{\circ}$. These are identified by CAL personnel as being due to specular reflections from the string support system. Thus they should not be construed as being characteristic of the patterns for model JULIET.

Special note should also be taken of those patterns obtained on FOXTROT and GOLF at DRTE at a frequency of 35,000 Mc (Figs. 8 and 13). Reference to Table I indicates that the average background return in the nose-on region in these cases is approximately the same as the average measured model return. Thus it is certain that the structure of the return at aspects less than 70° from nose-on is meaningless. It is also possible that the calculated average model cross section could be much higher than the actual value. Average cross-section values for these patterns have not been plotted on Fig. 21.

V. COMPARISON OF MEASURED DATA WITH APPROXIMATE THEORETICAL CALCULATIONS

Models FOXTROT, GOLF, and KING were designed to reduce traveling wave return. If this were accomplished in any degree, then the dominant contributor to the backscattering cross section of these models in the near nose-on region should be the creeping wave. (The other contributor, tip scattering, has a theoretical magnitude of about - 40 db λ^2 for these shapes--far below the measured nose-on cross sections.) Because of this, a rough calculation of the expected creeping wave return was made for comparison with the measured nose-on data.

The method used in this calculation involved the modification of the expression for the creeping wave magnitude for the sphere as given in van de Hulst:[6]

$$\frac{\sigma}{\lambda^2} = \frac{1}{4\pi}\left\{2.72\ (ka)^{4/3} \exp\left[-2.2\ (ka)^{1/3}\right]\right\}^2$$

where a is the sphere radius and $k = 2\pi/\lambda$. In order to modify this for use with FOXTROT, GOLF, and KING, it was assumed that the radius a in the factor $(ka)^{4/3}$ could be replaced by an average radius of curvature in the shadowed region, $\bar{\rho}$, and that πa in the exponent $(ka)^{1/3}$ represented loss due to path length and could thus be replaced by the distance, L, which the wave must travel in the shadowed region. We have then

$$\frac{\sigma_{creep}}{\lambda^2} = \frac{1}{4\pi}\left\{2.72\ (k\bar{\rho})^{4/3} \exp\left[-2.2\ (kL/\pi)^{1/3}\right]\right\}^2$$

Curves of near nose-on creeping wave cross section vs. a/λ, where, as before, a is the maximum body diameter, as calculated by this expression for FOXTROT, GOLF, and KING, are shown in Fig. 22. Values of exact nose-on measured cross section are shown as points. It is seen that several points, particularly for model KING (which theoretically has the lowest traveling wave return), lie close to the predicted curves. In general, however, the measured data show higher values than the predicted values, the largest discrepancies being in the FOXTROT data, where differences as high as 9 db are found. FOXTROT, of course, might still be expected to show a considerable traveling wave return, since there is still a finite discontinuity in curvature of the surface at the

junction of the ogival forward section and the spherical aft section. On the other hand, exact agreement could hardly be expected, since van de Hulst states that the expression used gives results apparently low by a factor of 2(~3 db) even in the sphere case. In fact, if the curves of Fig. 22 were to be raised by 3 db, it is seen that agreement with the measured data would, in general, be much better.

Predictions were also made for the exact aft end return, assuming that the specular return is dominant. For FOXTROT, GOLF, and KING, this was done using the geometrical optics formula

$$\sigma = \pi \rho^2$$

where ρ is the radius of curvature at the back end. For JULIET the prediction was made by calculating the return to be expected from a circular cylinder of length (L) equal to the circumference of JULIET at the aft end, and of radius (ρ) equal to the radius of curvature of the annular aft section. The formula used was Mentzer's physical optics expression[7]

$$\sigma = \frac{2\pi L^2 \rho}{\lambda}.$$

The predicted curves and the measured data are shown in Fig. 23. Agreement is only fair, with discrepancies as large as 4 db observed.

VI. CONCLUSIONS

It is apparent that the "low cross-section" shapes described in Section II have shown no significant reduction in average nose-on cross section over that of the cone-sphere. One reason for this in the cases of FOXTROT, GOLF, and KING is that most measurements have been made only in the region $a/\lambda < 3$, in which the creeping wave dominates the cone-sphere return. Thus, reduction in traveling wave return over that of the cone-sphere would not be easily detectable for these measurements.

The measurements on JULIET indicated that the re-entrant back end of this model did not noticeably reduce the creeping wave return.

Additional measurements at values of $a/\lambda > 3$ would be useful and may possibly show a considerable reduction in the average cross sections of these shapes over that of the cone-sphere.

Comparison of the measured data with theoretical predicted data shows satisfactory agreement, considering the crudeness of the approximations involved.

REFERENCES

1. R. E. Kleinman, T.B.A. Senior, "Studies in Radar Cross Sections XLVIII - Diffraction and Scattering by Regular Bodies - II: The Cone", University of Michigan, Radiation Laboratory, January, 1963.

2. D. L. Moffatt, "Low Radar Cross-Sections, the Cone-Sphere", Ohio State University Research Foundation, Report No. 1223-5, 15 May 1962.

3. J. H. Pannell, J. Rheinstein, A. F. Smith, to be published.

4. E. M. Kennaugh, D. L. Moffatt, "On the Axial Echo Area of the Cone-Sphere Shape", Proc. IRE 50 (1962), p. 199.

5. W. E. Blore, "Experimental Measurements of the Radar Cross Section of a Cone Sphere", Proc. IEEE 51 (1963), p. 1263.

6. H. C. van de Hulst, Light Scattering by Small Particles, J. Wiley and Sons, Inc., New York (1957), p. 371.

7. J. R. Mentzer, Scattering and Diffraction of Radio Waves, Pergamon Press, London and New York (1955), p. 108.

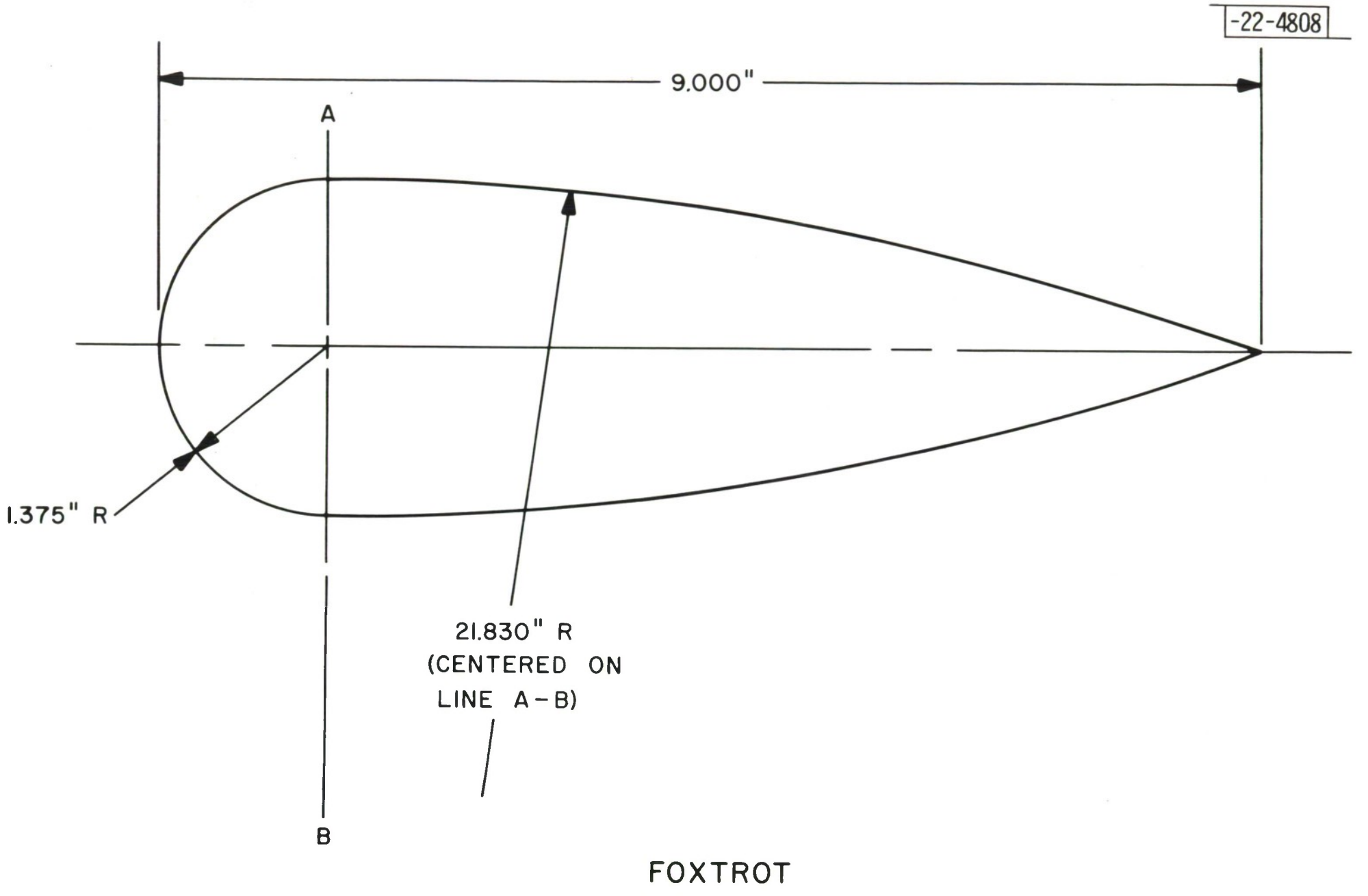

Figure 1: Model FOXTROT

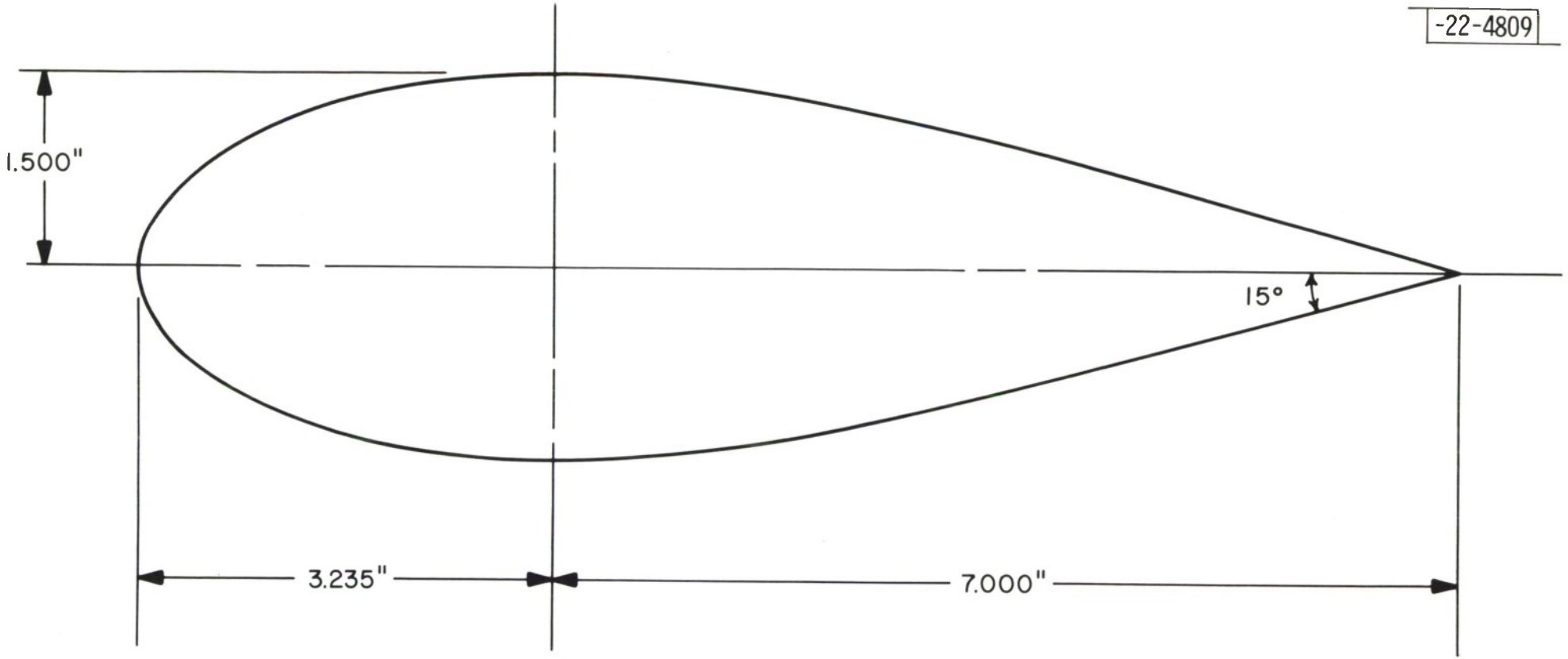

GOLF

Figure 2: Model GOLF

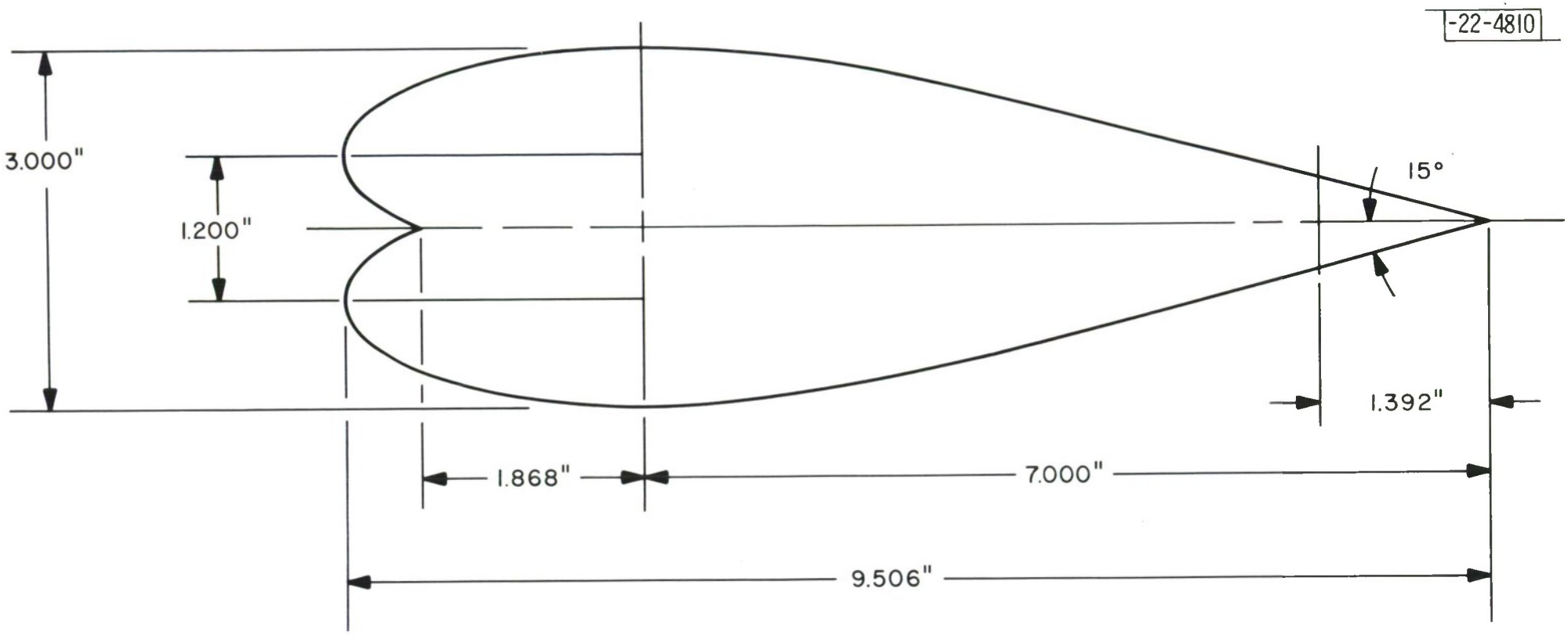

JULIET

Figure 3: Model JULIET

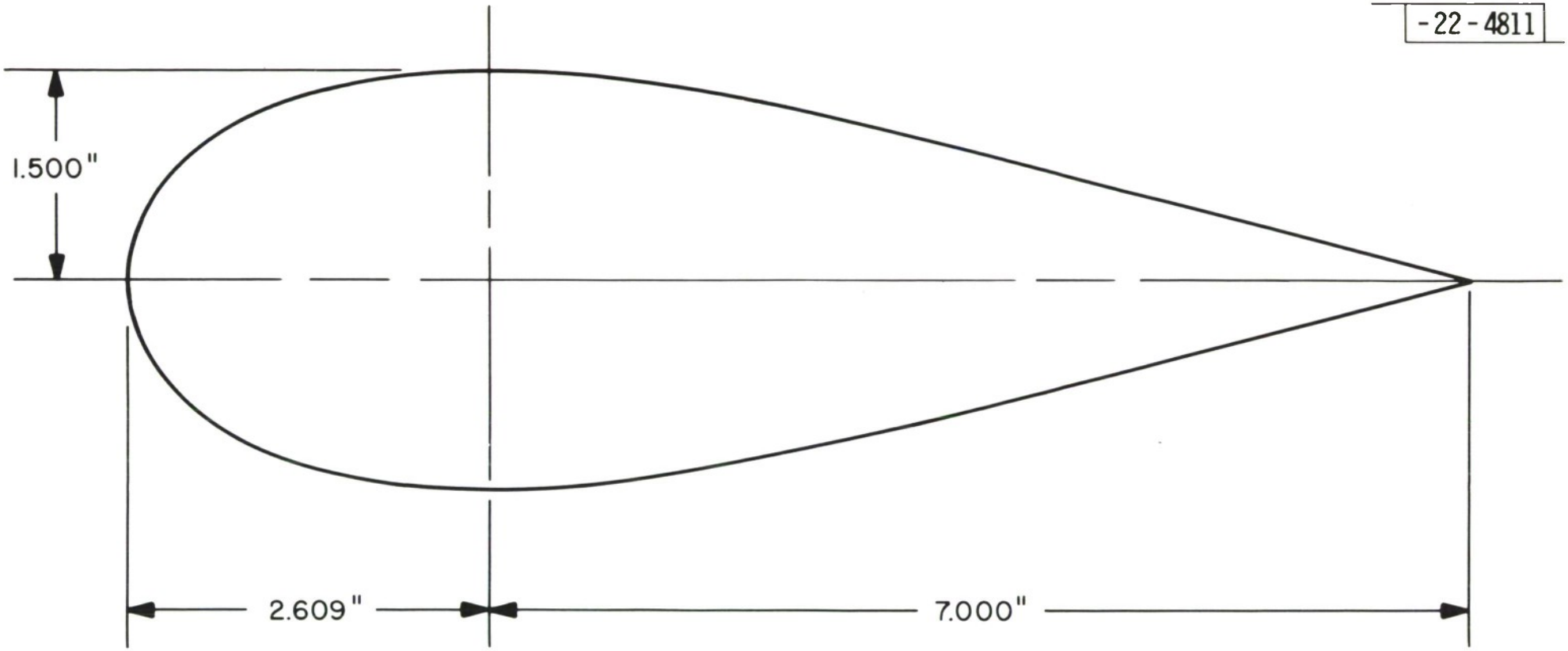

KING

Figure 4: Model KING

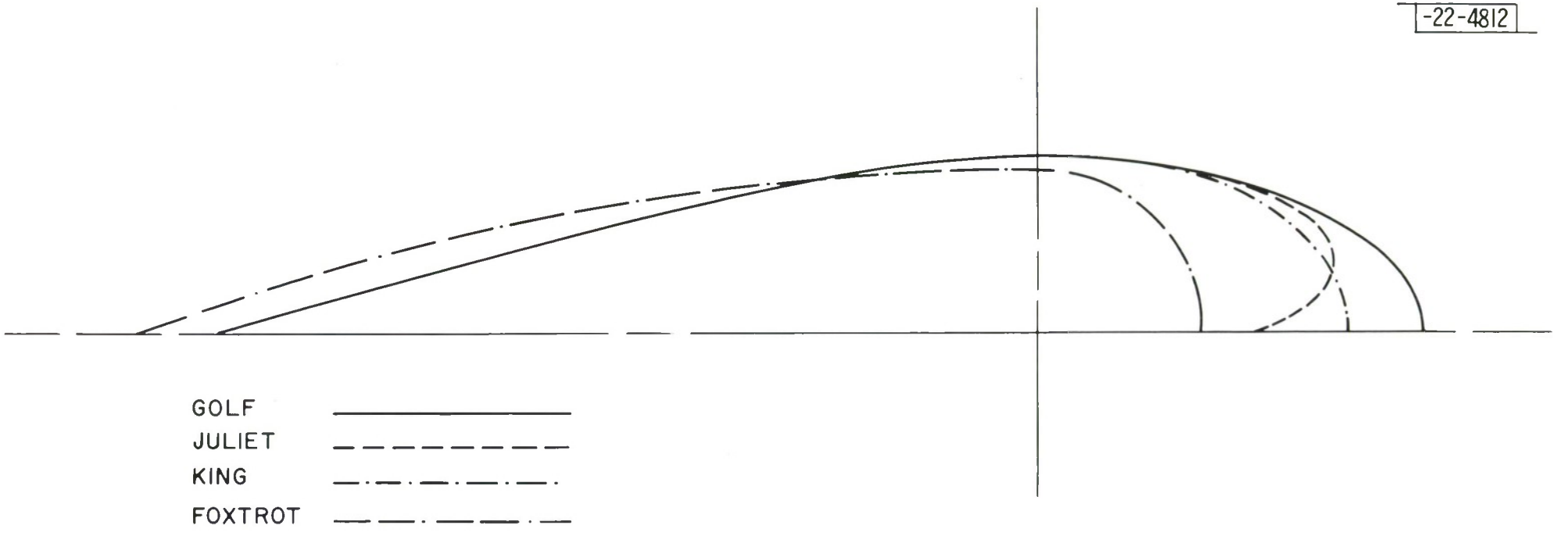

Figure 5: Comparison of Shapes

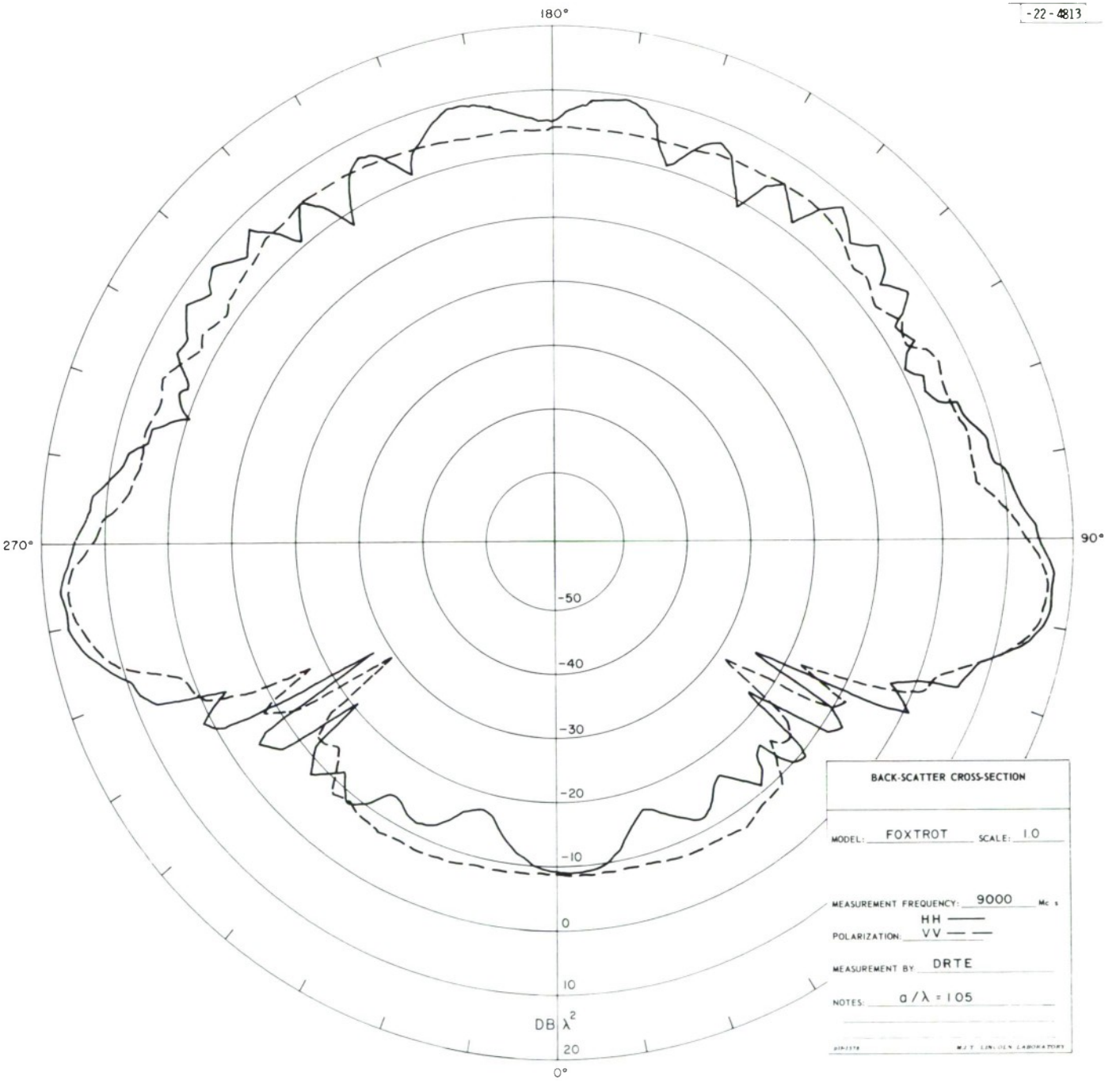

Figure 6: Backscattering Pattern, Model FOXTROT, $a/\lambda = 1.05$

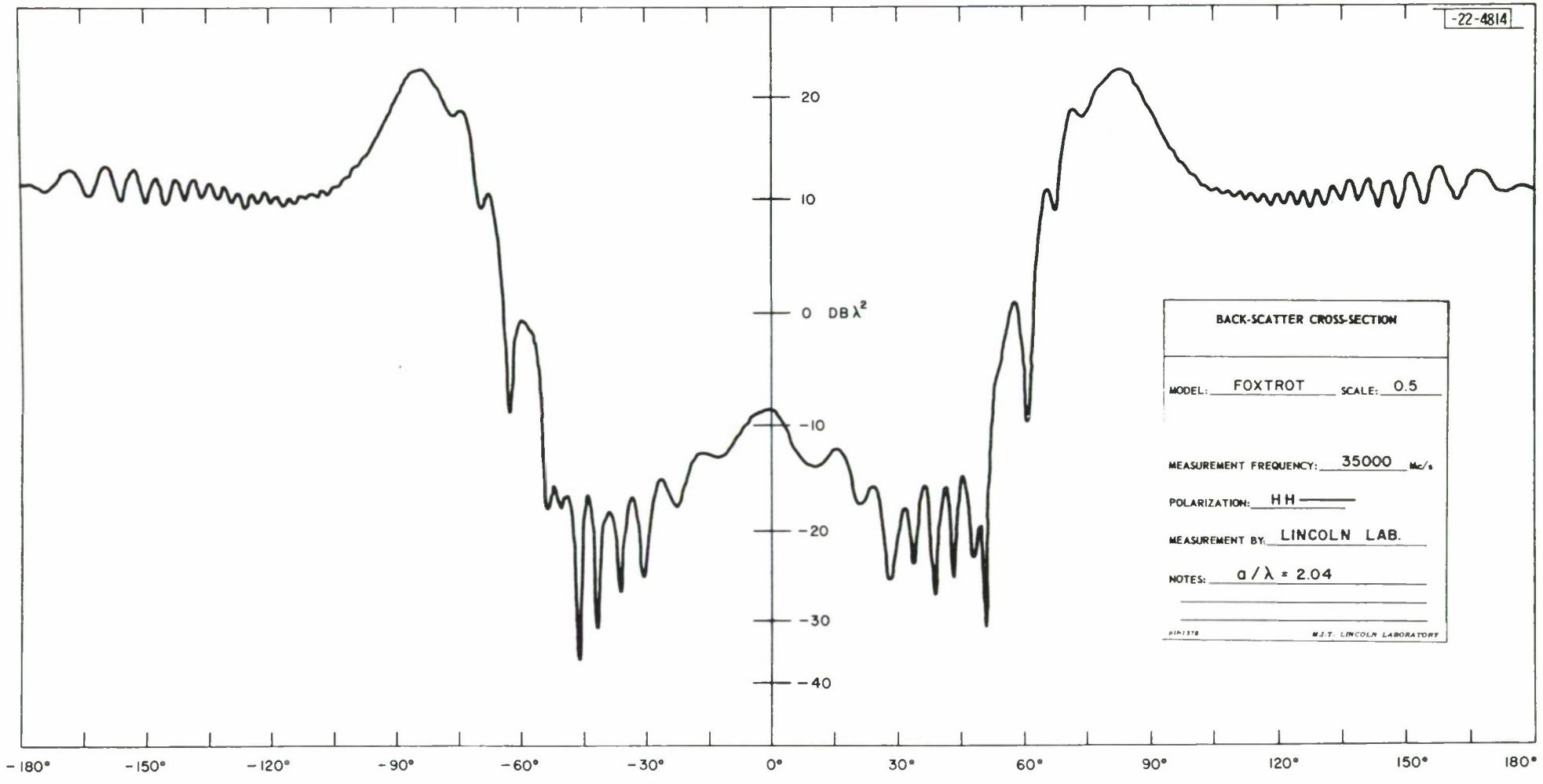

Figure 7: Backscattering Pattern, Model FOXTROT, $a/\lambda = 2.04$

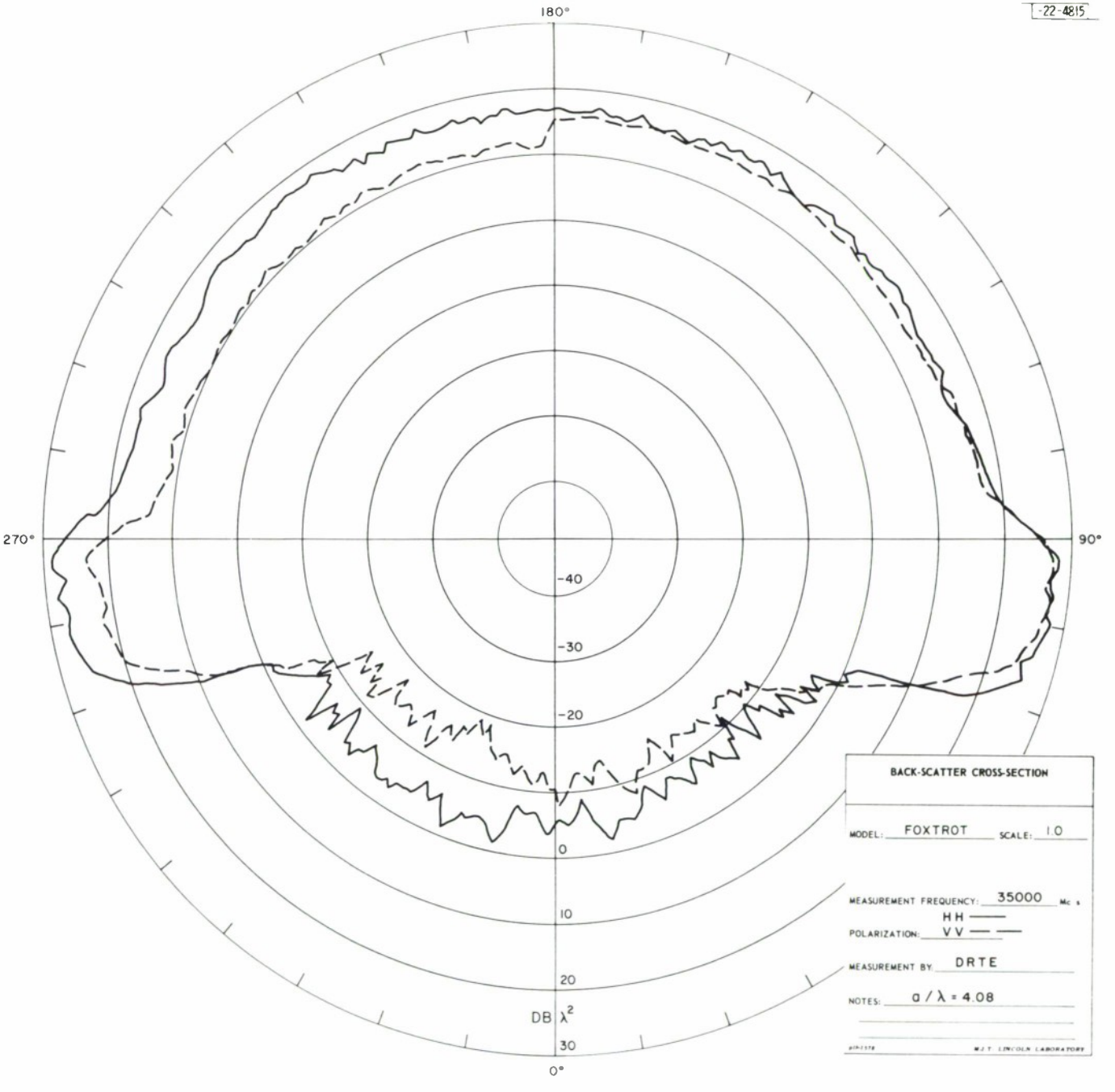

Figure 8: Backscattering Pattern, Model FOXTROT, $a/\lambda = 4.08$

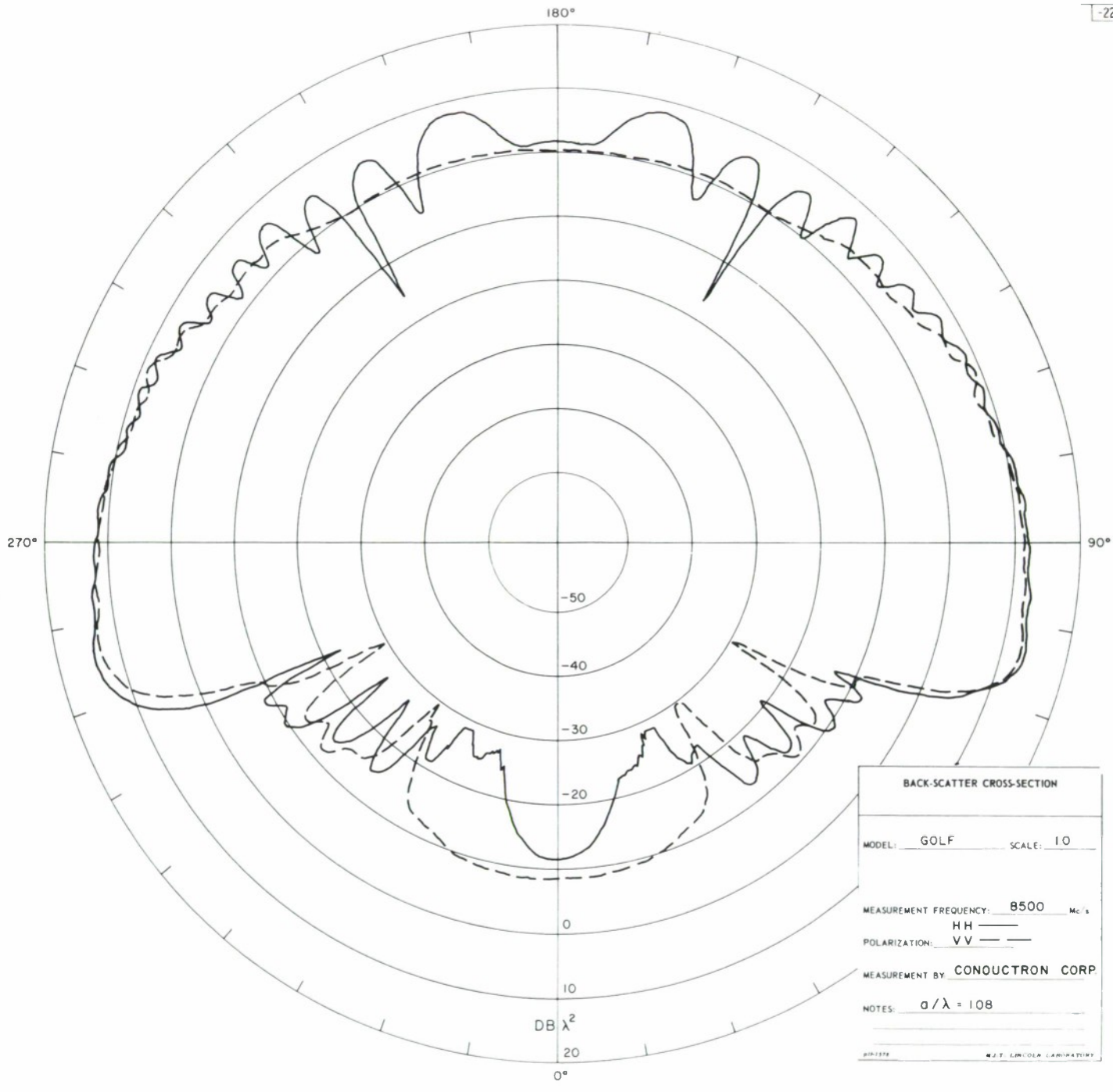

Figure 9: Backscattering Pattern, Model GOLF, $a/\lambda = 1.08$

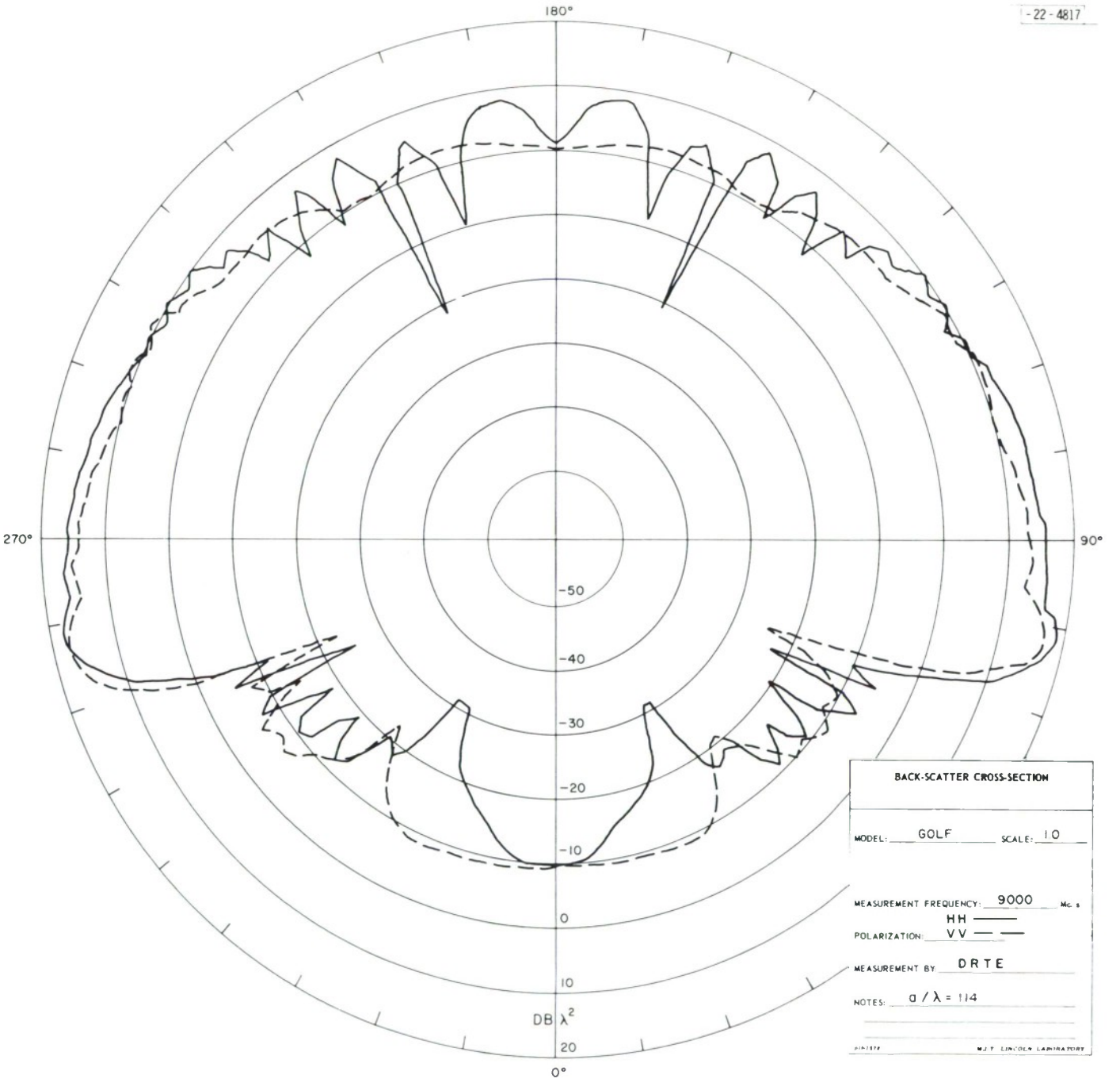

Figure 10: Backscattering Pattern, Model GOLF, $a/\lambda = 1.14$

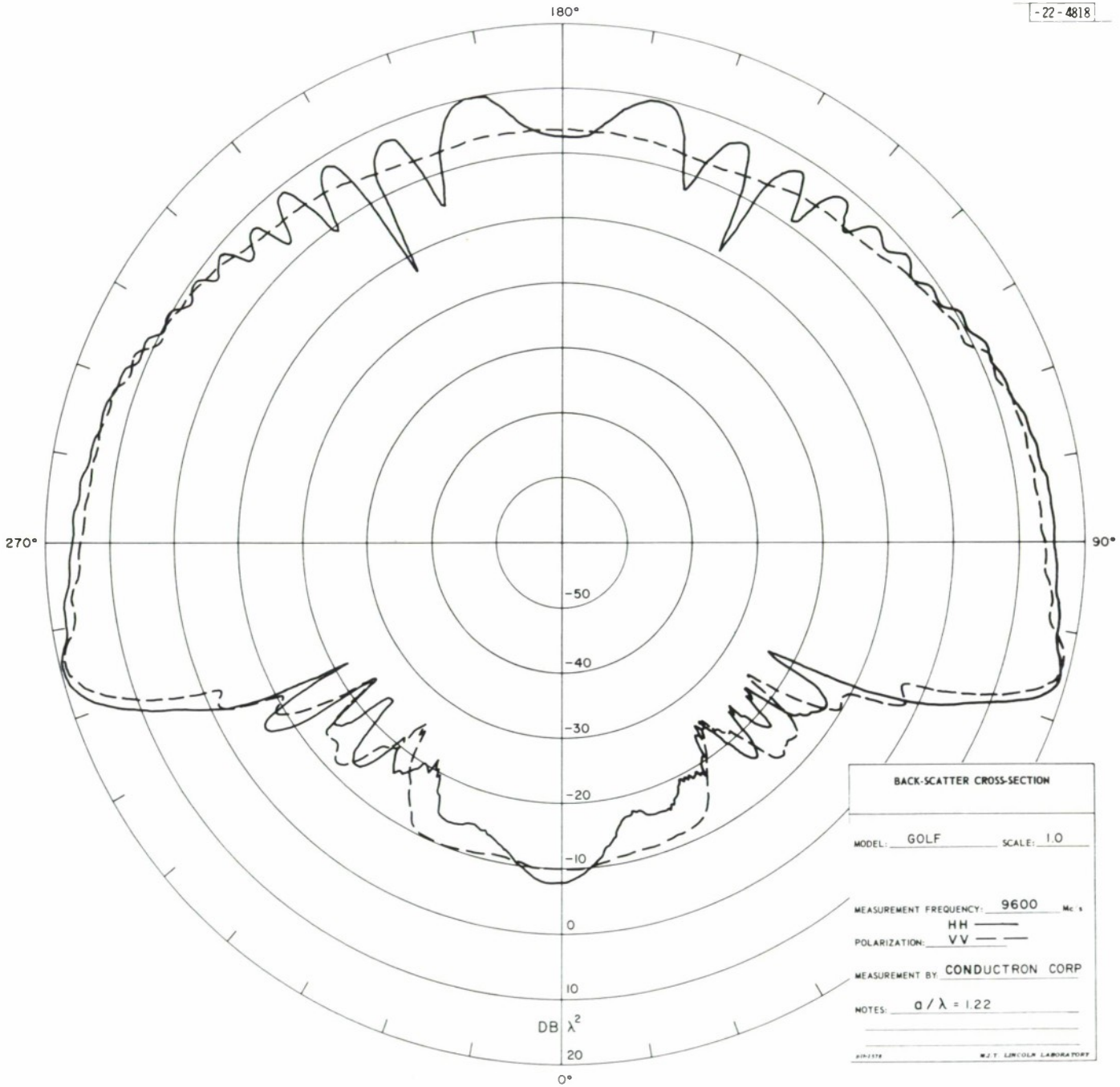

Figure 11: Backscattering Pattern, Model GOLF, $a/\lambda = 1.22$

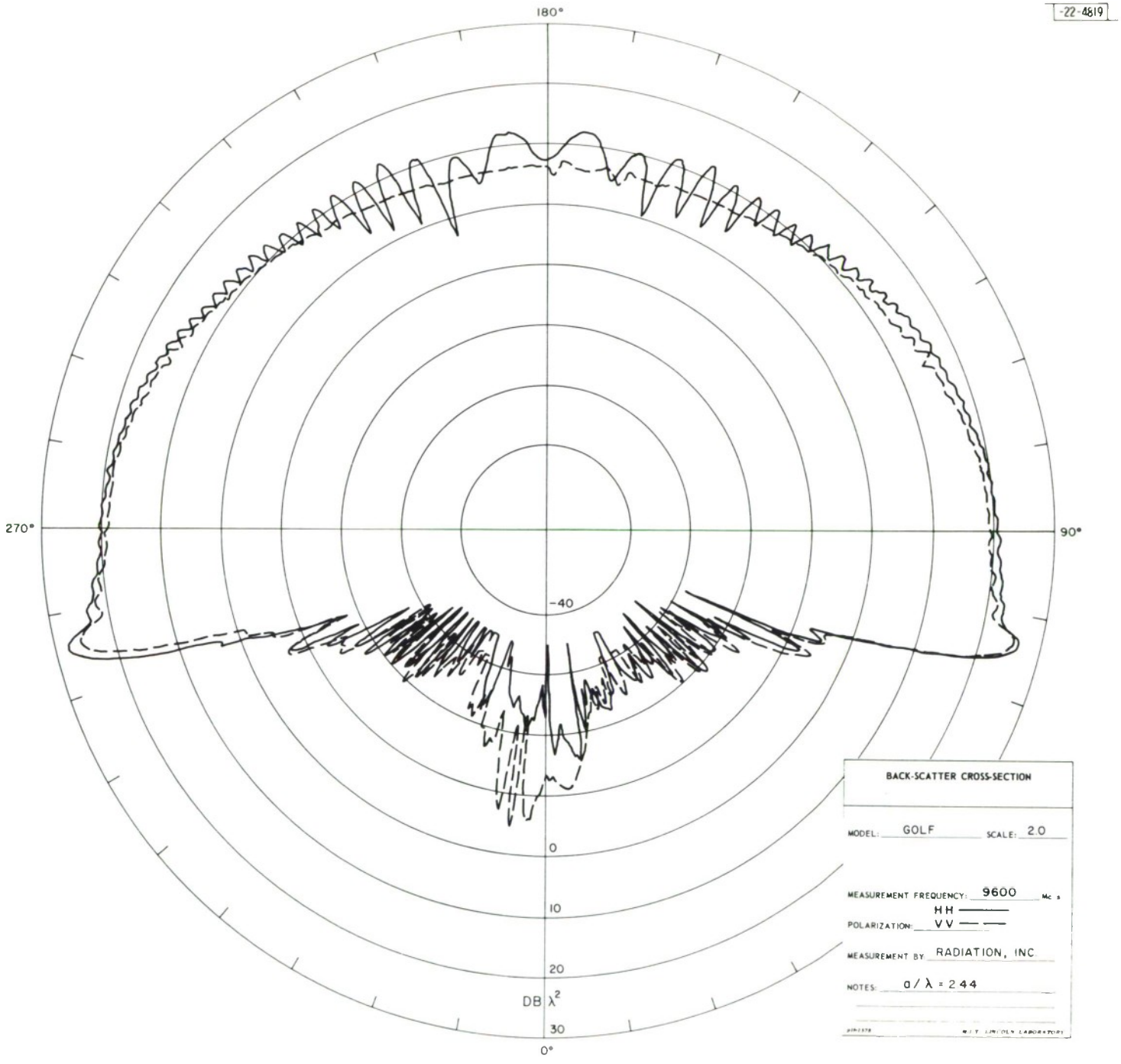

Figure 12: Backscattering Pattern, Model GOLF, $a/\lambda = 2.44$

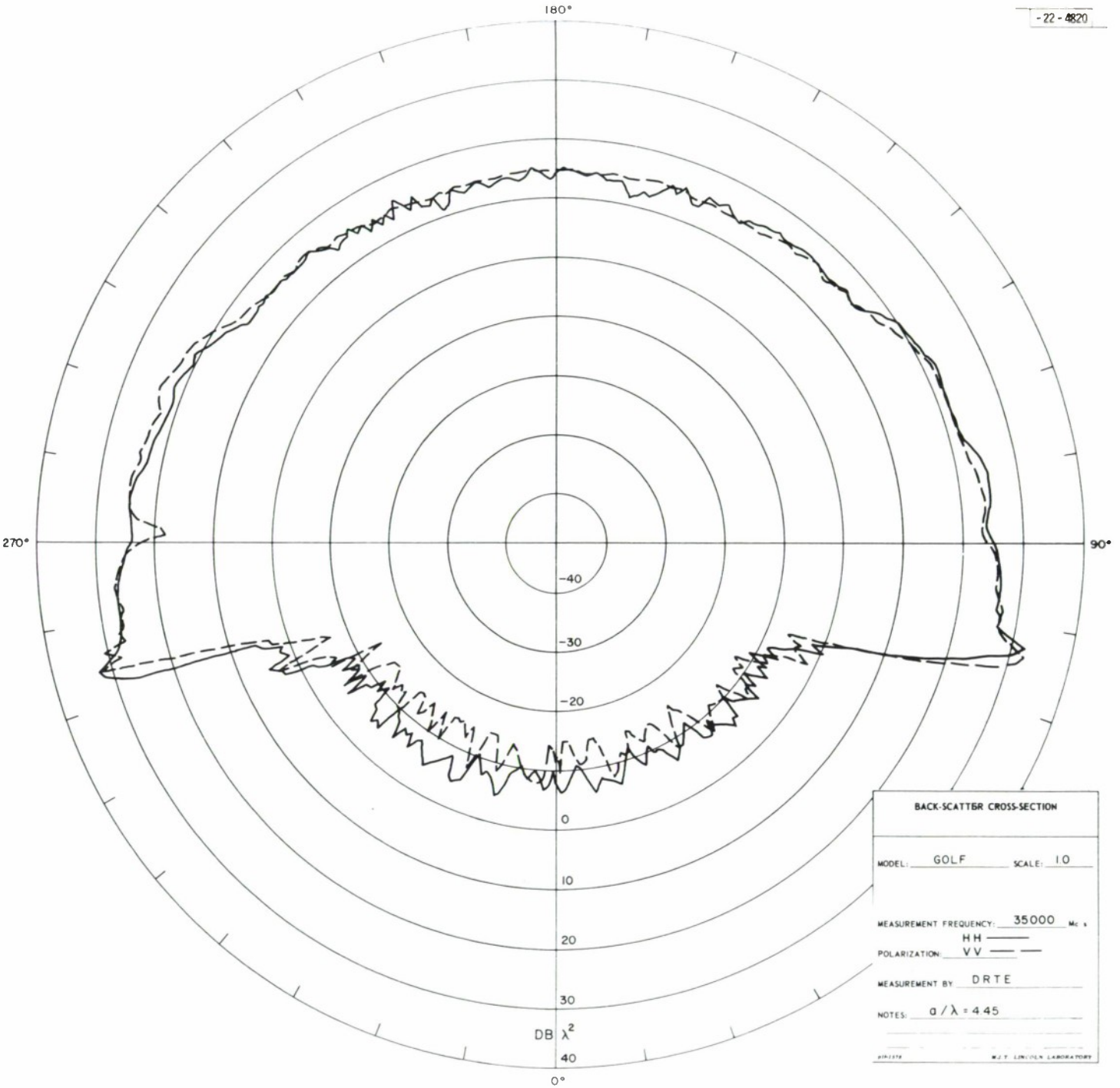

Figure 13: Backscattering Pattern, Model GOLF, $a/\lambda = 4.45$

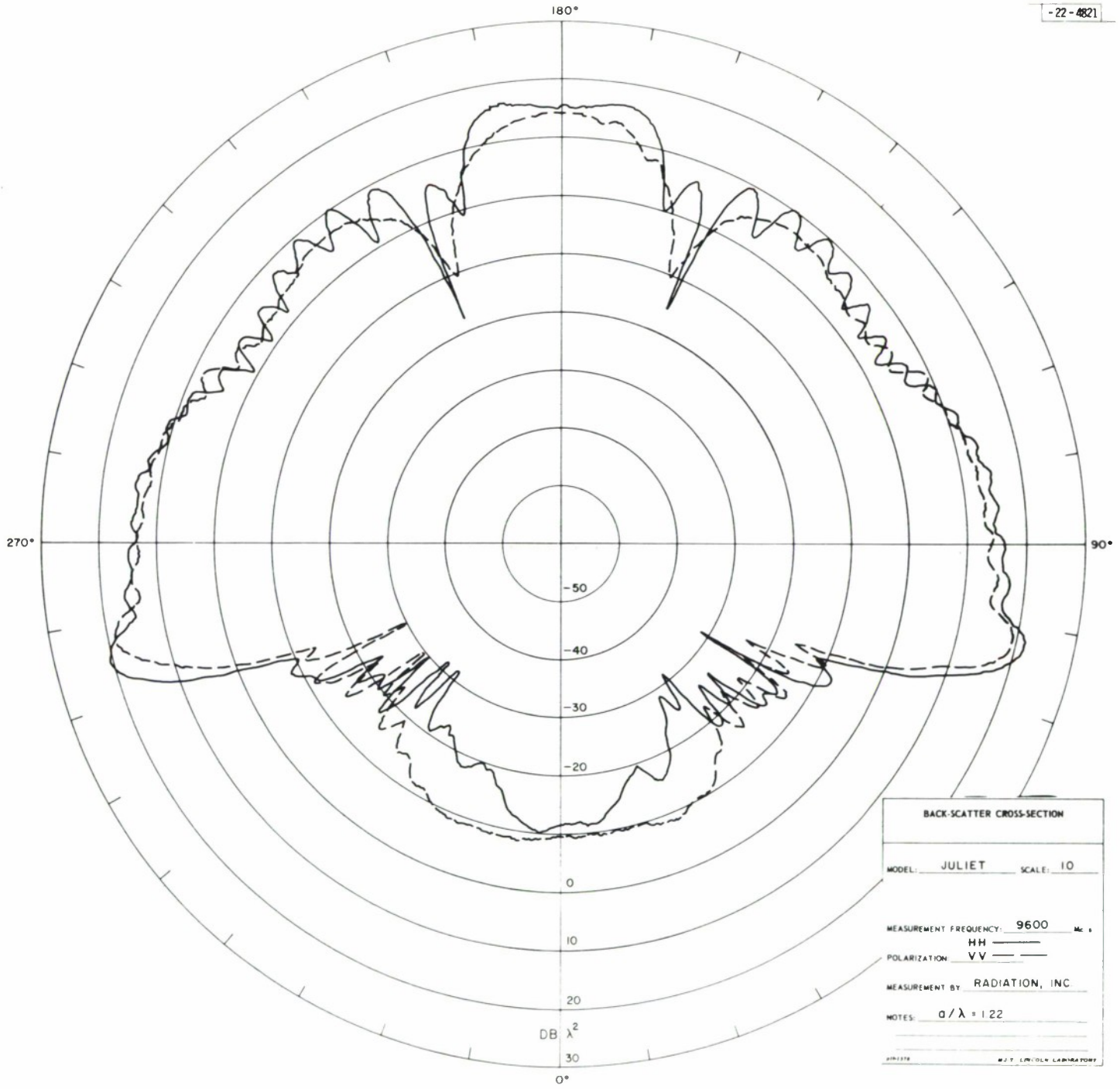

Figure 14: Backscattering Pattern, Model JULIET, $a/\lambda = 1.22$

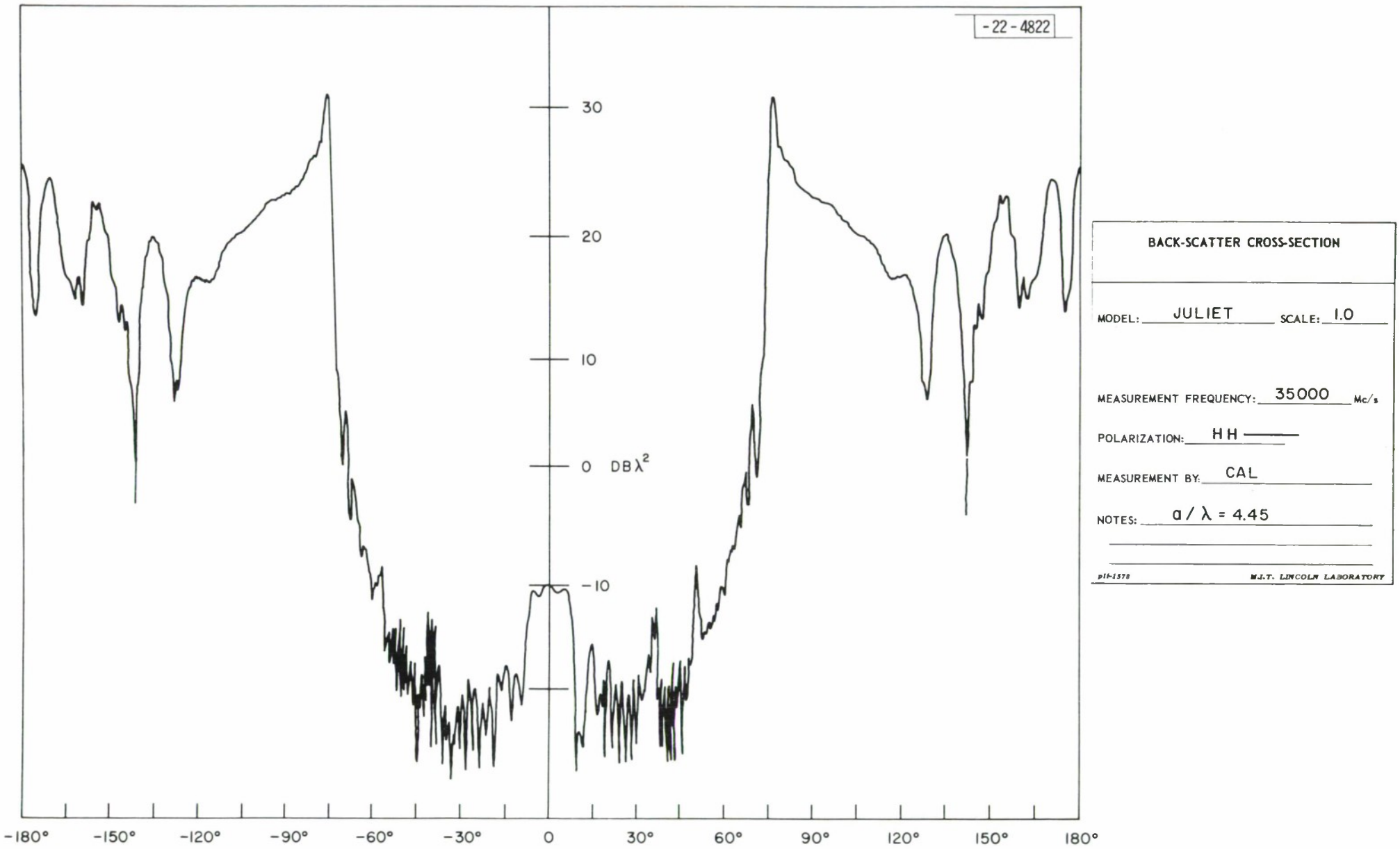

Figure 15: Backscattering Pattern, Model JULIET, $a/\lambda = 4.45$ (HH pol.)

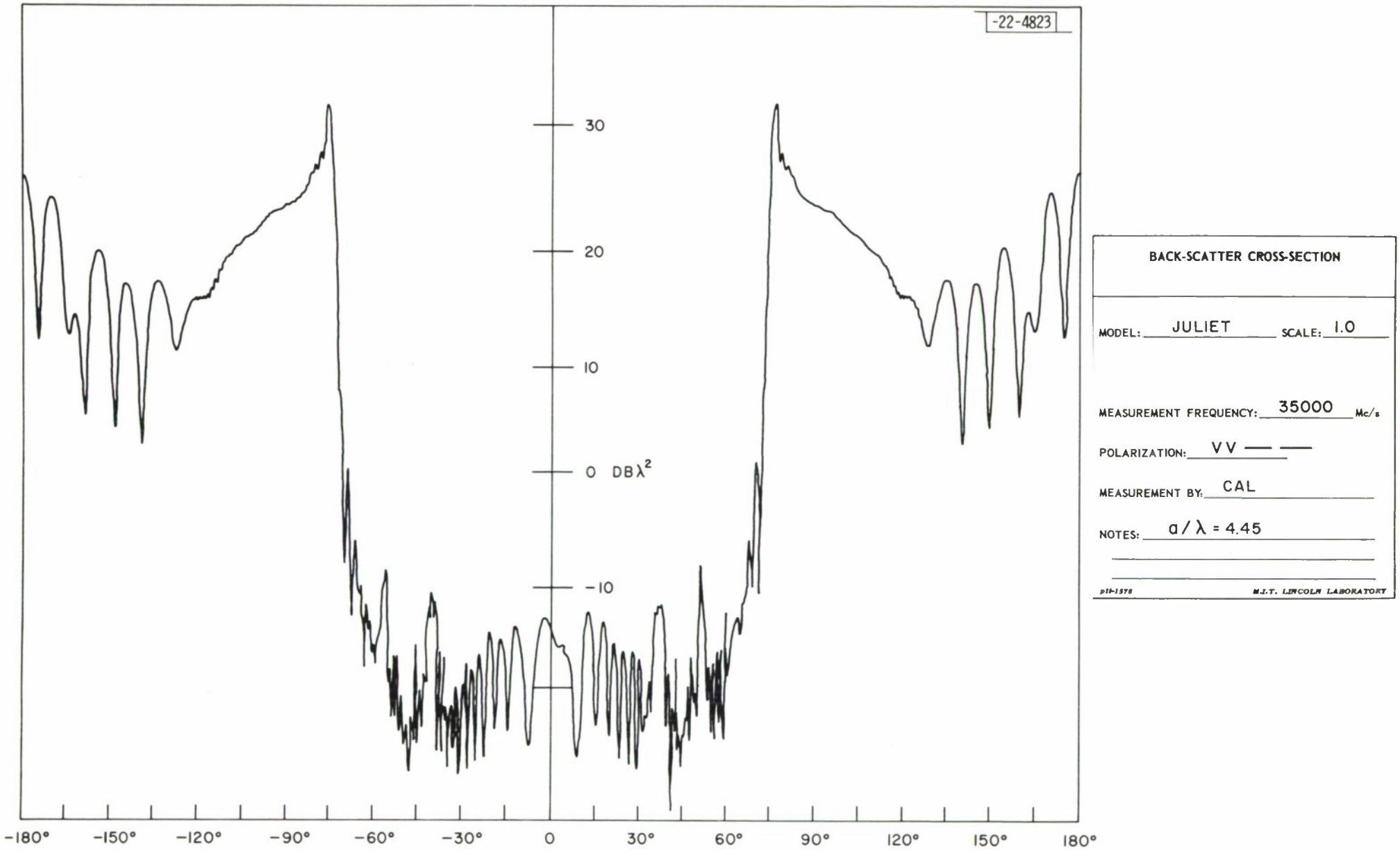

Figure 16: Backscattering Pattern, Model JULIET, $a/\lambda = 4.45$ (VV pol.)

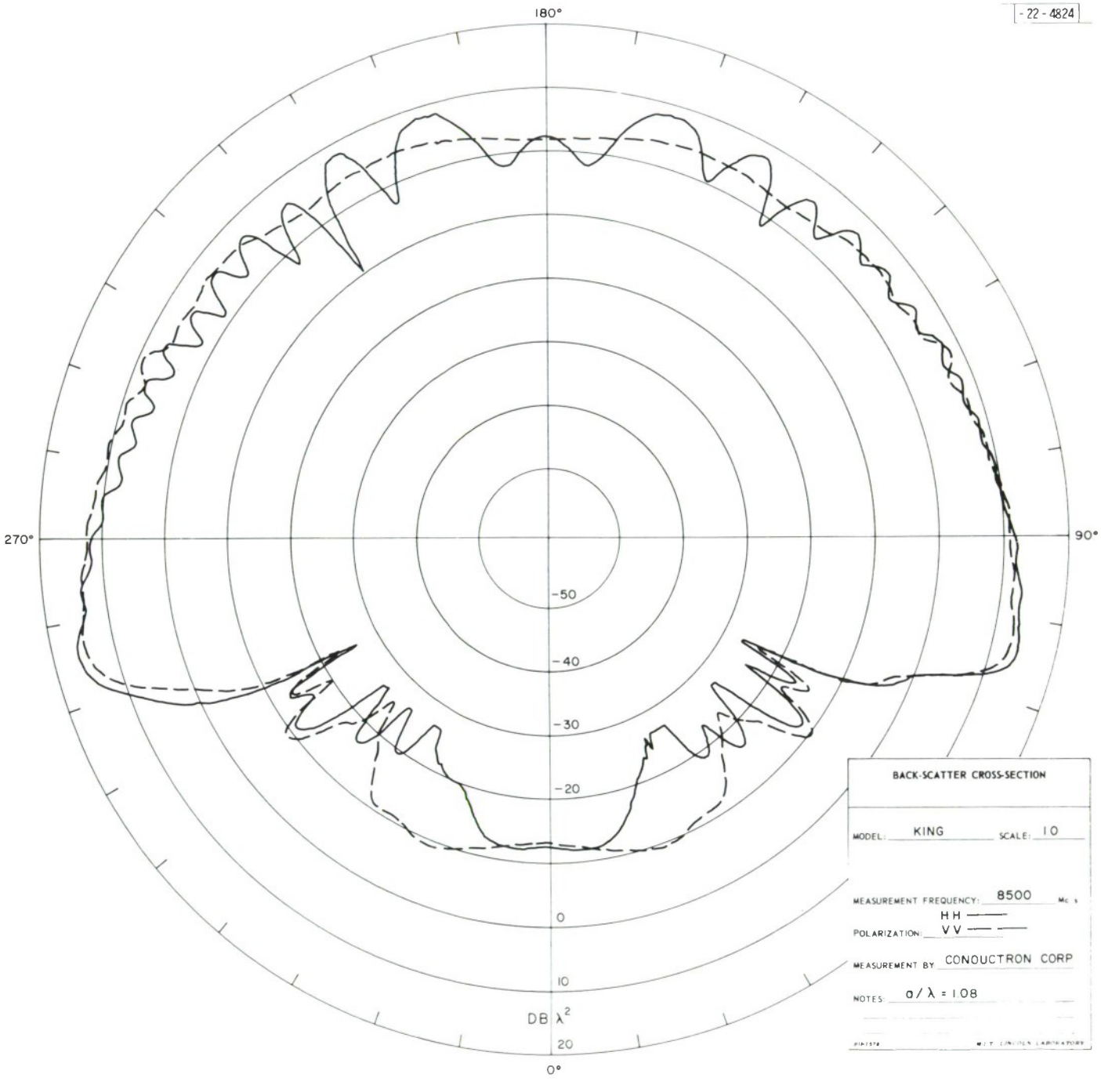

Figure 17: Backscattering Pattern, Model KING, $a/\lambda = 1.08$

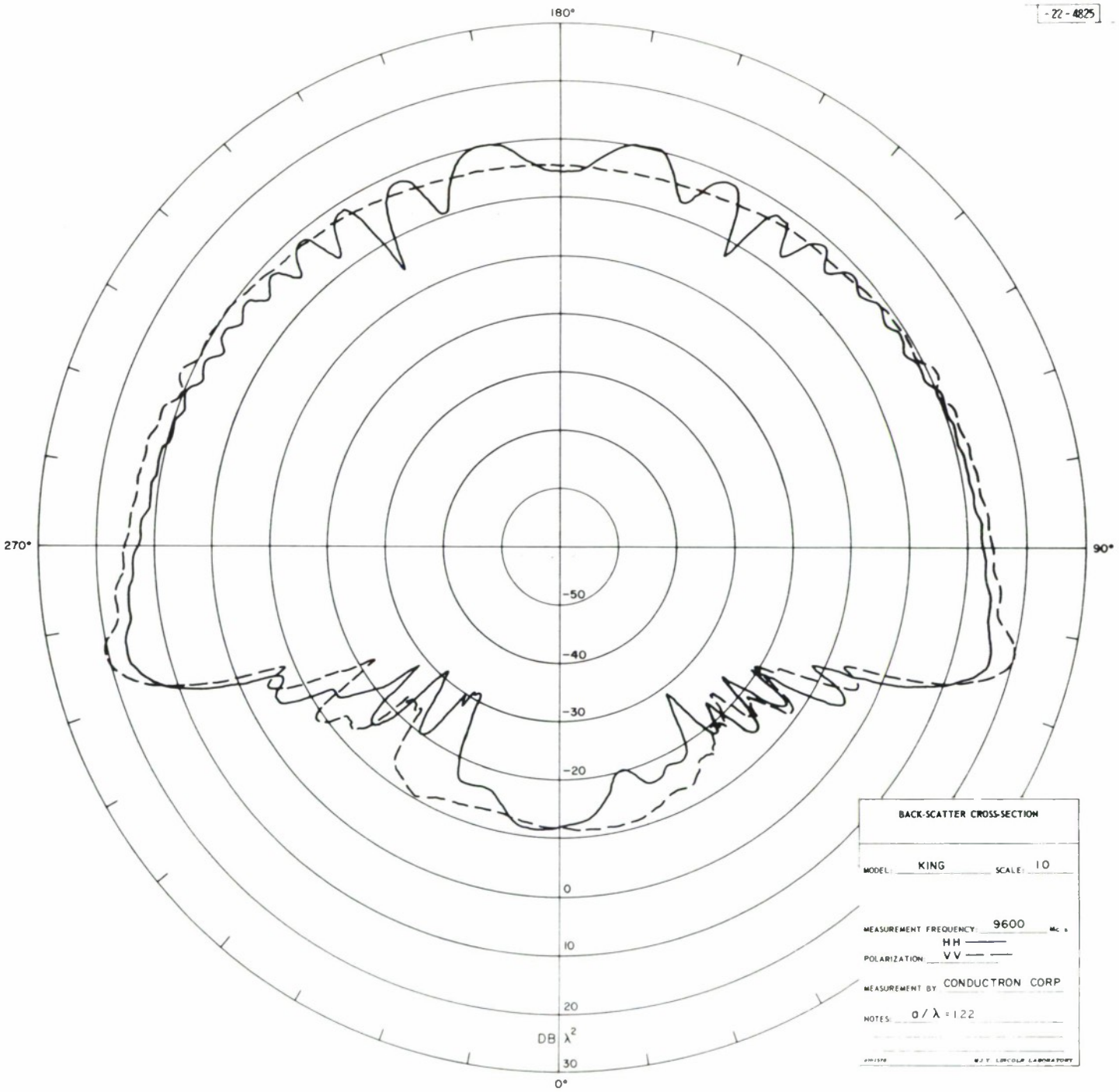

Figure 18: Backscattering Pattern, Model KING, $a/\lambda = 1.22$ (Cond.)

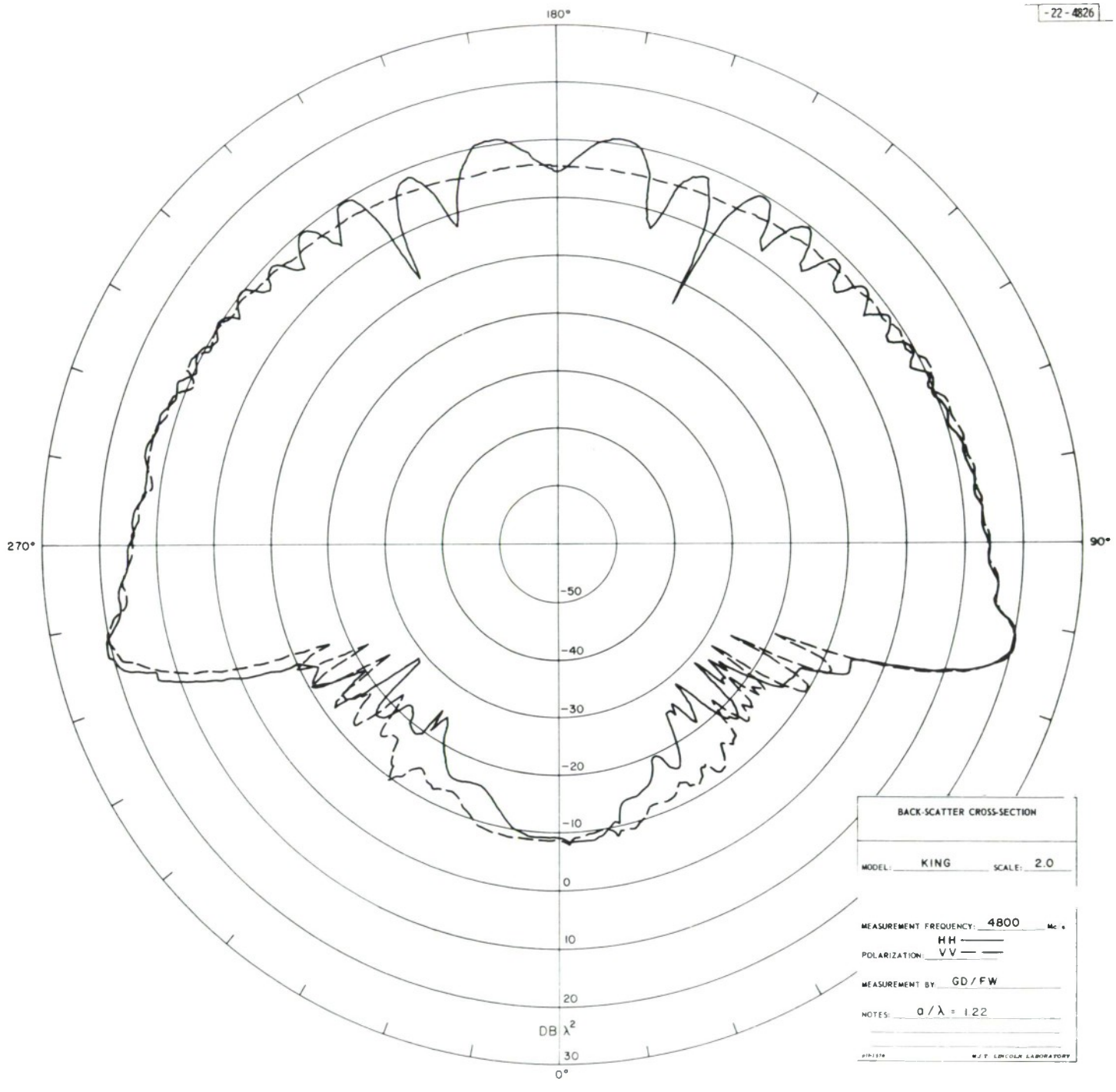

Figure 19: Backscattering Pattern, Model KING, $a/\lambda = 1.22$ (GD/FW)

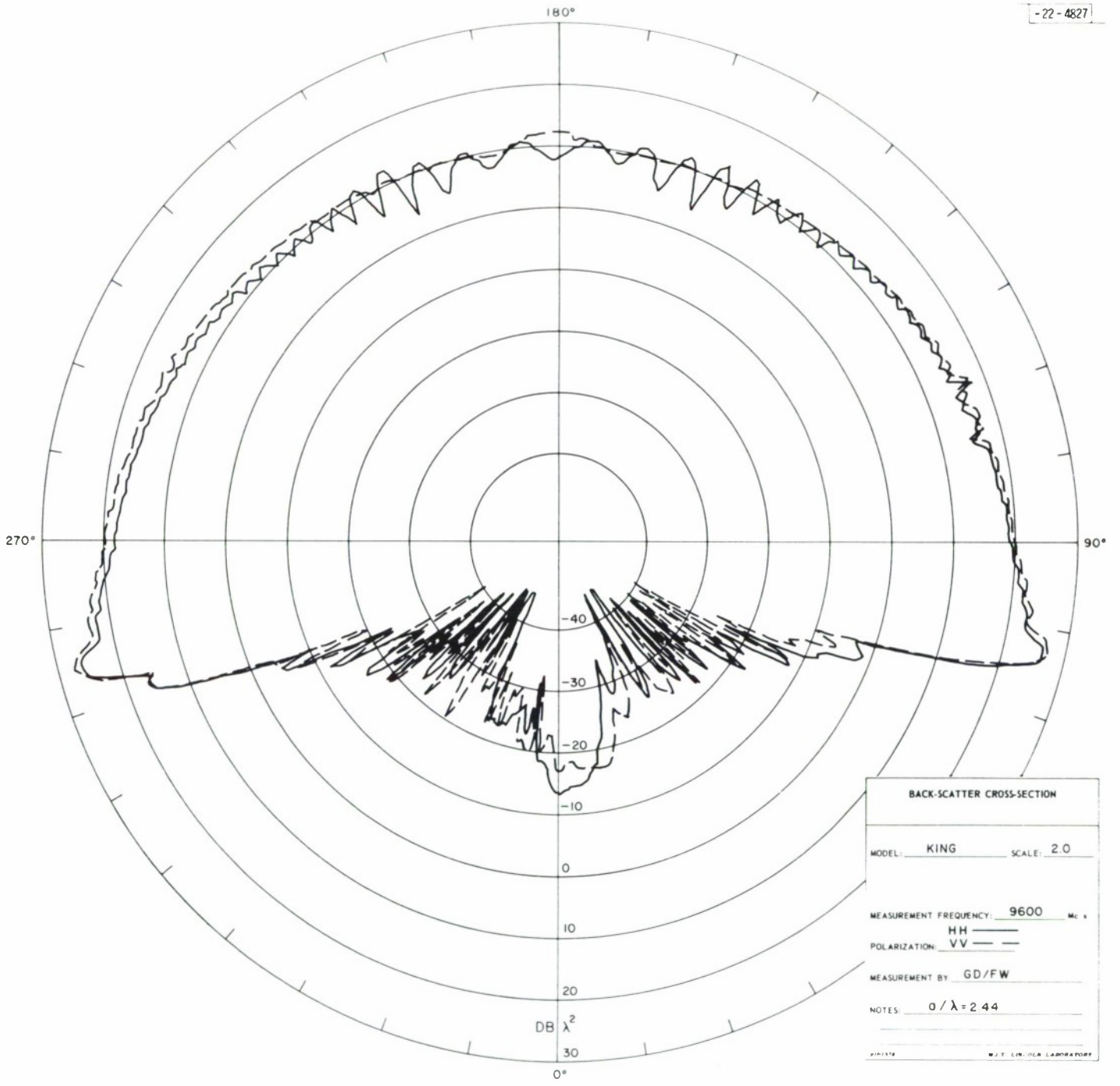

Figure 20: Backscattering Pattern, Model KING, $a/\lambda = 2.44$

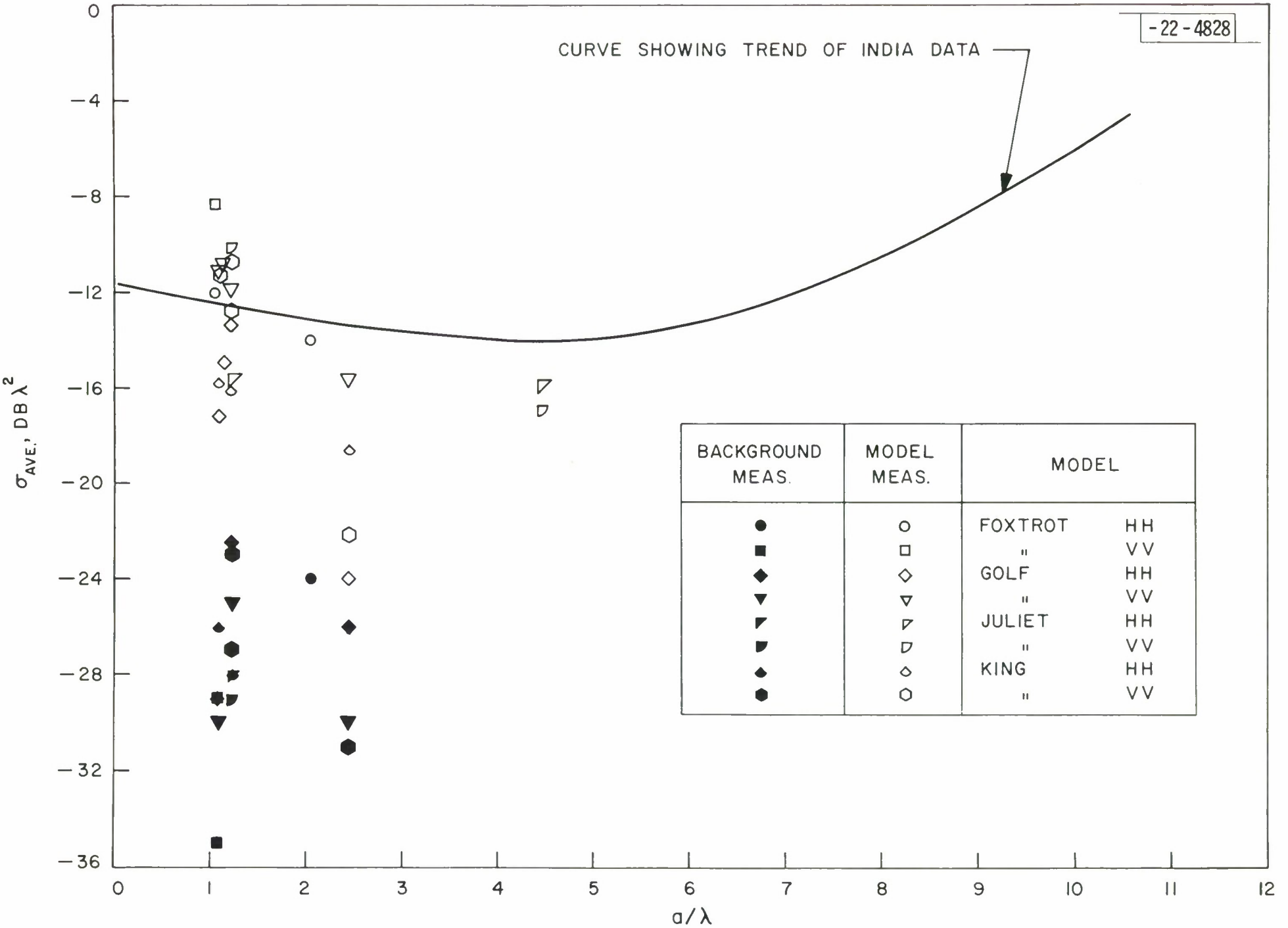

Figure 21: Average Nose-on Return vs. a/λ

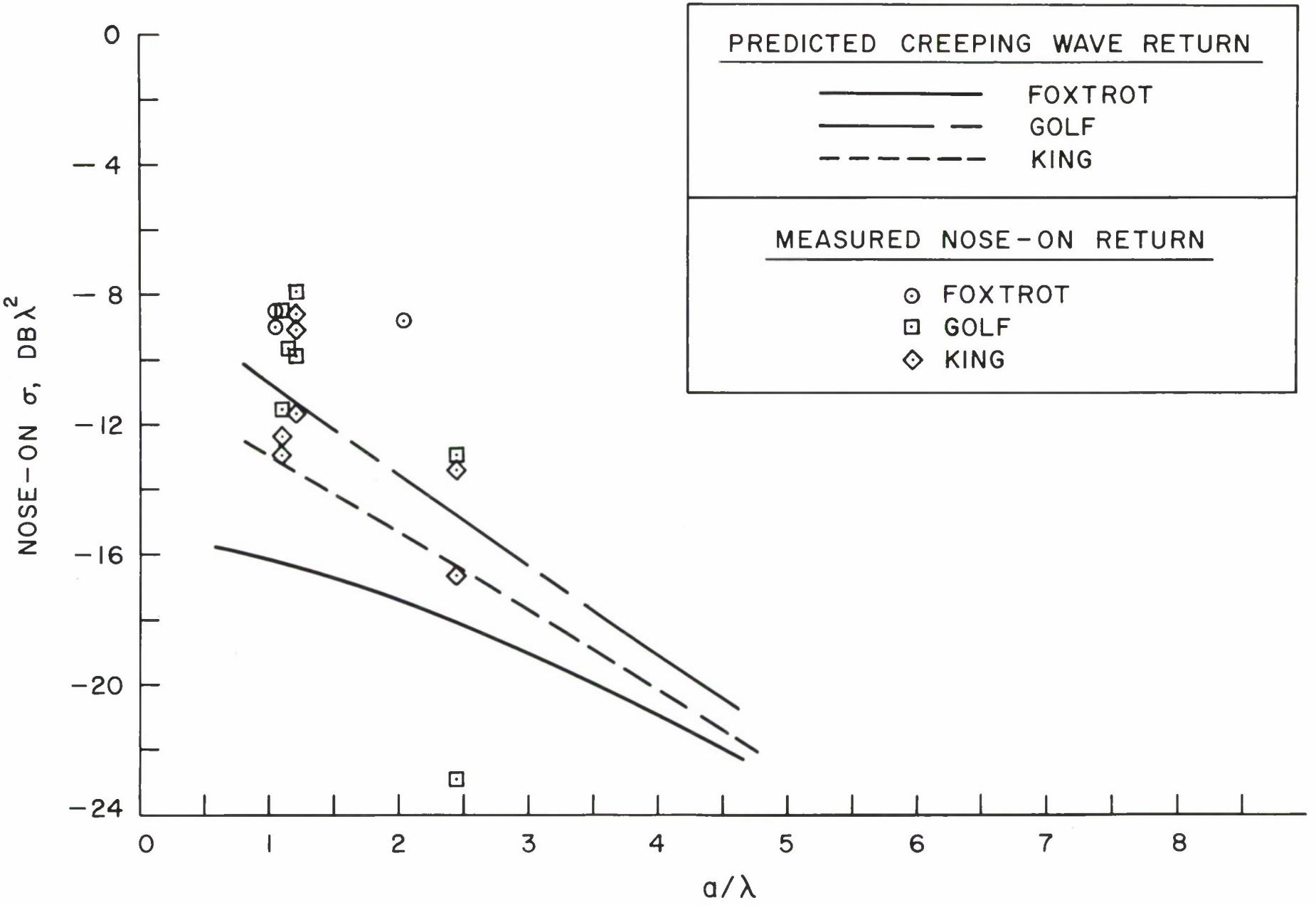

Figure 22: Creeping Wave Return vs. a/λ

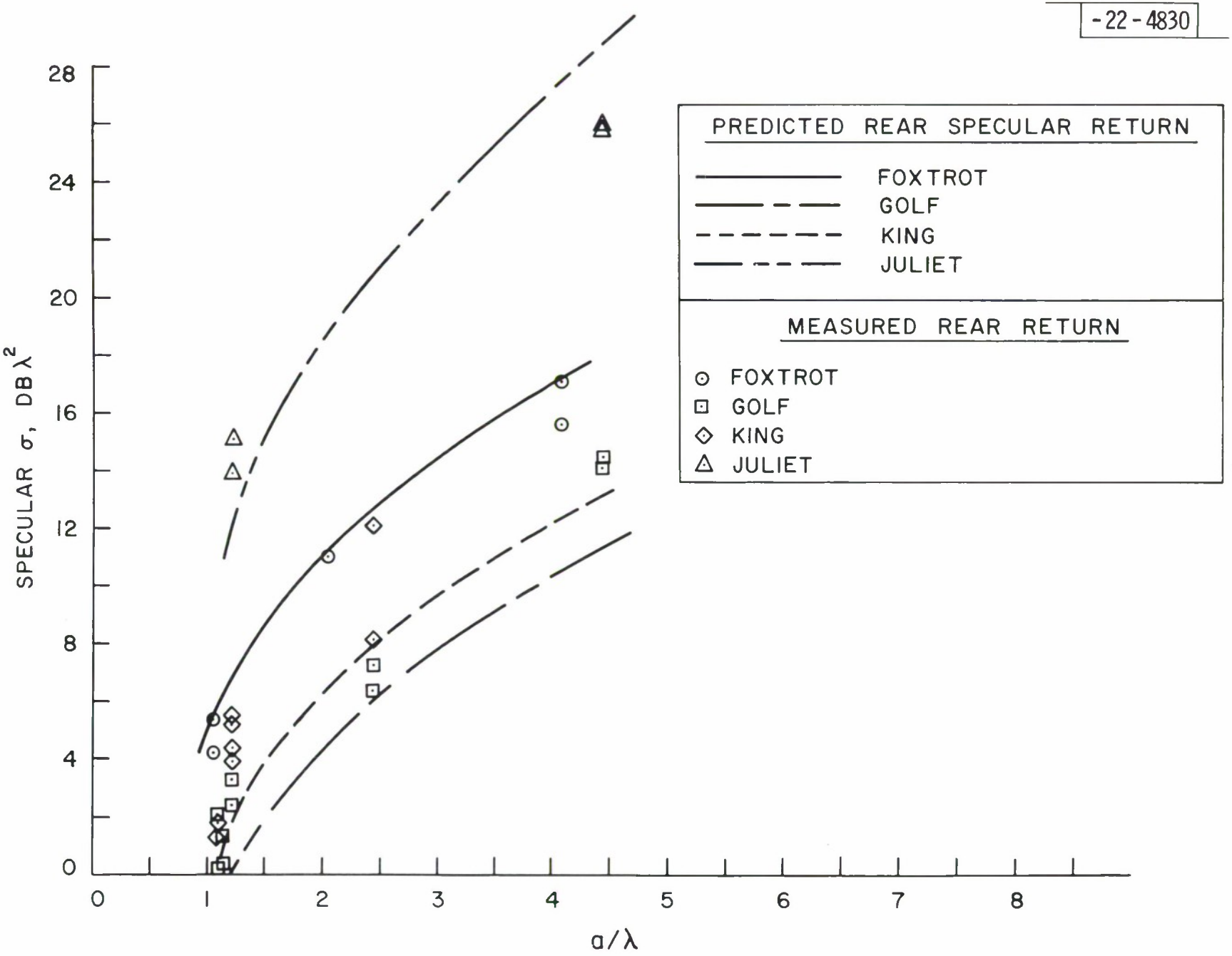

Figure 23: Back End Return vs. a/λ